

Measurements of Powder–Polymer Mixture Properties and Their Use in Powder Injection Molding Simulations for Aluminum Nitride

KUNAL H. KATE,¹ VALMIKANATHAN P. ONBATTUVELLI,² RAVI K. ENNETI,³ SHI W. LEE,⁴ SEONG-JIN PARK,⁵ and SUNDAR V. ATRE^{1,6}

1.—Oregon State University, Corvallis, OR 97331, USA. 2.—Intel Corporation, Chandler, AZ 85226, USA. 3.—Global Tungsten Powders, Towanda, PA 18848, USA. 4.—Pusan National University, Busan, Republic of Korea. 5.—Pohang University of Science and Technology, Pohang, Republic of Korea. 6.—e-mail: sundar.atre@oregonstate.edu

Aluminum nitride has been favored for applications in manufacturing substrates for heat sinks due to its elevated temperature operability, high thermal conductivity, and low thermal expansion coefficient. Powder injection molding is a high-volume manufacturing technique that can translate these useful material properties into complex shapes. In order to design and fabricate components from aluminum nitride, it is important to know the injection-molding behavior at different powder–binder compositions. However, the lack of a materials database for design and simulation at different powder–polymer compositions is a significant barrier. In this paper, a database of rheological and thermal properties for aluminum nitride–polymer mixtures at various volume fractions of powder was compiled from experimental measurements. This database was used to carry out mold-filling simulations to understand the effects of powder content on the process parameters and defect evolution during the injection-molding process. The experimental techniques and simulation tools can be used to design new materials, select component geometry attributes, and optimize process parameters while eliminating expensive and time-consuming trial-and-error practices prevalent in the area of powder injection molding.

INTRODUCTION

Powder injection molding (PIM) is useful to economically net-shape complex ceramic and metal components at high production volumes. In PIM, ceramic or metal powder is compounded with polymer (binder) and used to mold parts with an injection-molding machine, in a manner analogous to the fabrication of conventional thermoplastics. Subsequently, the polymer is removed (debinding) from the molded part and then sintered under controlled time, temperature, and atmospheric conditions to get the final part of desired dimensions, density, microstructure, and properties. Due to the requirement for several subsequent processing steps, it is essential to identify appropriate powder–binder mixture (feedstock) compositions and processing conditions that will result in obtaining parts that are free of defects such as weld lines, internal

stresses, cracks, and warpage during the injection-molding stage. One common approach to resolve precision and defect avoidance issues during manufacturing is to lower the amount of powder in the powder–polymer mixture to improve the mold filling attributes and increase the green strength during ejection of the part from the mold. However, the volume fraction of powder not only affects powder–polymer mixture properties and molding behavior but also the debinding and sintering conditions as well as the final dimensions of the part.

Equation 1 provides the final dimensions of the sintered part based on the initial volume fraction of powder, ϕ_p .¹

$$Y = 1 - \left(\frac{\phi_p}{f_s} \right)^{\frac{1}{3}} \quad (1)$$

where Y is the linear shrinkage factor and f_s is the fractional sintered density. This inter-relationship

between component shrinkage, sintered density, and initial volume fraction of powder is shown in Fig. 1. It can be seen that parts with lower volume fraction of powder in the feedstock undergo larger shrinkage for a given sintered density. Sintering to lower final density is typically not an option since structural and functional properties depend on achieving high sintering densities. Alternatively, mold cavity dimensions can be changed to achieve the desired sintered dimensions, but that would involve expensive and time-consuming tool rework. Therefore, there is a critical need to address the effects of feedstock composition on the injection-molding attributes and defect avoidance at the component design stage itself.

Several injection-molding simulation platforms are available for addressing the above design challenges in PIM. In order to facilitate the design of PIM components using such simulation tools, there is a critical need to determine the effects of variation in material composition on the thermal, rheological, and mechanical properties of powder–polymer mixtures. The experimental data that are typically required for powder–polymer mixtures at high volume fractions of powder are limited in the literature and tend to be expensive to obtain for specific volume fractions of powder.

In order to understand the effects of compositional changes on powder–polymer mixture properties, empirical models that have a limited number of fitting constants to predict feedstock properties were evaluated and used in the current study using aluminum nitride (AlN) PIM feedstocks. The approach involved using experimental property data of the unfilled polymer and a powder–polymer mixture at 0.52 volume fraction AlN powder in conjunction with the selected mixing models to model a number of physical properties over a range of powder volume fractions in the feedstock. The

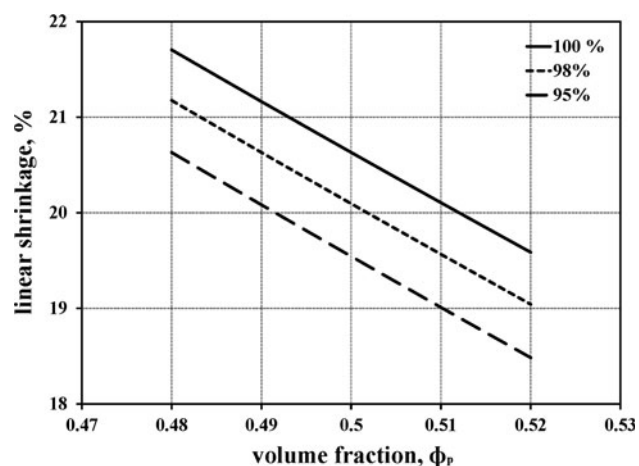


Fig. 1. Dependence of linear shrinkage on final sintered density and different volume fractions of powder, ϕ_p .

modeled data thus generated were used as input into a feedstock property file in the Moldflow Insight software (Autodesk, Inc., San Rafael, CA) for simulating the injecting-molding process. These simulations were used to understand the sensitivity of feedstock composition and consequently, physical properties on the injection-molding behavior and defect evolution in AlN components. It is anticipated that the experimental techniques and modeling and simulation tools presented in this study can be generalized to design new materials, select component geometry attributes, and optimize process parameters while eliminating expensive and time-consuming trial-and-error practices prevalent in PIM.

EXPERIMENTAL MATERIALS AND METHODS

Commercially available AlN ($D_{50} \sim 1 \mu\text{m}$) and Y_2O_3 ($D_{50} \sim 50 \text{ nm}$) were used as the starting materials in as-received condition. The micrographs of the powder was taken with the Quanta field-emission gun (FEI Company, Hillsboro, OR) dual-beam scanning electron microscope (SEM) coupled with an energy dispersive x-ray spectrometer (EDAX Inc., Mahwah, NJ) and is shown in Fig. 2. A total of 5 wt.% Y_2O_3 was added on the basis of AlN to the powder mixture. A multicomponent binder system consisting of paraffin wax, polypropylene, polyethylene-g-maleic anhydride (LDPE-g-MA), and stearic acid (SA) was used in the current study. Details of the composition and mixing preparations are provided elsewhere.² Torque rheometry was performed in the Intelli-Torque Plasticorder (Brabender GmbH, Duisburg, Germany) in order to determine the maximum packing density of the powder–polymer mixture. Twin-screw extrusion of

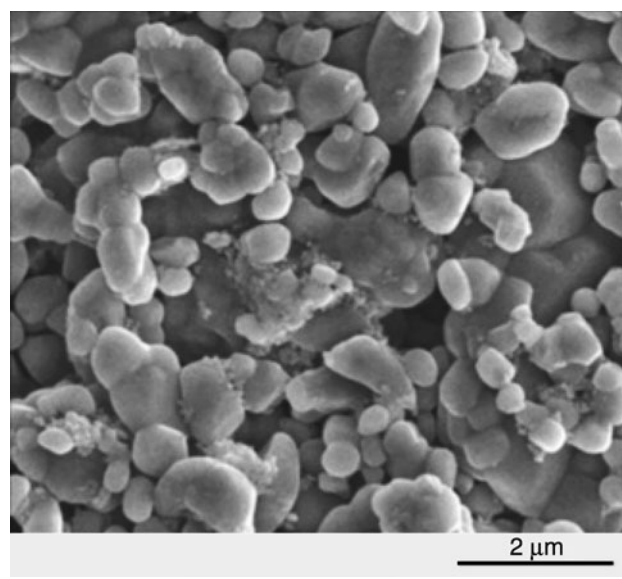


Fig. 2. SEM images of AlN powder used in this study.

AlN feedstocks was performed with an Entek corotating 27-mm twin-screw extruder (Entek Manufacturing, Lebanon, OR) with an L/D ratio of 40 and pelletized for further use. Injection molding was performed on an Arburg 221M injection-molding machine (Arburg, Lossburg, Germany). Thermogravimetric analysis was performed on the extruded feedstocks using TA-Q500 (TA Instruments, New Castle, DE) thermal system operated under nitrogen flow in the temperature range of 50°C to 600°C with a heating rate of 20°C/min in order to confirm the powder weight fraction in the feedstock.

The rheological characteristics of the feedstock were examined on a Rheograph 2003 capillary rheometer (Göttfert, Buchen, Germany) at different shear rates and temperatures. The testing was carried out in accordance with ASTM D 3835. The temperatures were between the highest melting temperature and the lowest degradation temperature of the binder system. The barrel of inner diameter of 1 mm and die length of 20 mm was used. The preheating time was kept at 6 min. A K-System II Thermal Conductivity System was used to evaluate the thermal conductivity of the feedstock. The testing was carried out in accordance with ASTM D 5930. The initial temperature was 190°C and final temperature was 30°C. The probe voltage was kept at 4 V and acquisition time of 45 s. Specific heat measurements were carried out on PerkinElmer DSC7 equipment (PerkinElmer, Waltham, MA) in accordance with ASTM E 1269. The testing was done with an initial temperature of 190°C and final temperature of 20°C. The cooling rate was kept constant of 20°C/min. A Gnomix pressure-volume-temperature (PVT) apparatus was used to find the PVT relationships of the feedstock materials. The test was carried out in accordance with ASTM D 792. The pellets were dried for 4 h at 70°C under vacuum. The measurement type used was isothermal heating scan with a heating rate of approximately 3°C/min.

Autodesk Moldflow Insight 2011 software was used for simulating the injection conditions of two heat-sink geometries. The heat-sink geometries were built using Autodesk Solidworks 2011 software and the geometry was imported in Moldflow Insight software. The part was meshed using an automated solid three-dimensional meshing, which makes use of finite-element analysis for meshing. The process settings were 303 K for the mold temperature and 433 K for the melt temperature. Simulations were conducted for a fill-and-pack type condition in order to meet the objective of understanding injection-molding behavior and its packing characteristics.

ESTIMATING PROPERTIES OF POWDER-POLYMER MIXTURES

The experimentally determined physical properties of AlN powder-polymer mixtures at 0 and 0.52

volume fraction were used to estimate properties of AlN powder-polymer mixtures with 0.48–0.51 volume fractions. In order to estimate these properties, various models were initially screened before choosing models that were specific to estimating material properties at high volume fraction fillers. Further, models having fewer empirical constants were preferred over alternatives, when necessary. Additionally, the viscosity and PVT data required curve fitting to extract constants required for the simulations using Autodesk Moldflow Insight software.

Density

The melt and solid density of powder-polymer mixtures can be estimated using various models.^{3,4} In this article, an inverse rule-of-mixtures was used⁴ as given in Eq. 2

$$\frac{1}{\rho_c} = \frac{X_b}{\rho_b} + \frac{X_p}{\rho_p} \quad (2)$$

where ρ is the density, X is the mass fraction, and the subscripts c, b, and p stand for the composite, binder, and powder respectively. Furthermore, the mass fractions for powder and binder can be calculated using Eq. 3.

$$X_p = \frac{\phi_p \rho_p}{\phi_p \rho_p + \phi_b \rho_b} \quad X_b = \frac{\phi_b \rho_b}{\phi_p \rho_p + \phi_b \rho_b} \quad (3)$$

where ϕ is the volume fraction of the powder. A comparison of density as a function of volume fraction of powder is shown in Table I. The melt and solid density data for 0 and 0.52 volume fractions ϕ_p were experimentally obtained, while the values for intermediate volume fractions were estimated using Eq. 2. It was observed that for a change from 0 to 0.52 volume fraction of AlN, the melt density increased from 727 kg/m³ to 1969 kg/m³, and the solid density increased from 879 kg/m³ to 2252 kg/m³. The data in Table I indicate a $\pm 2\%$ variation in melt and solid density as a result of a $\pm 4\%$ change in the volume fraction of AlN.

Table I. Comparison of melt and solid densities for different volume fractions of AlN powder, ϕ_p

Volume Fraction (ϕ_p)	Melt Density (kg/m ³)	Solid Density (kg/m ³)
0	727	879
0.48	1873	2128
0.49	1897	2152
0.5	1921	2177
0.51	1945	2201
0.52	1969	2225

Table II. Specific heat capacity values at various temperatures for different volume fractions of AlN powder, ϕ_p

Volume Fraction (ϕ_p)	Temperature (K)						
	283	298	304	322	331	374	423
	Specific Heat Capacity C_p (J/kg·K)						
0	2080	3360	3840	4900	4640	3490	2530
0.48	960	1190	1460	2890	1200	1200	1260
0.49	950	1170	1440	2870	1170	1180	1250
0.5	940	1150	1420	2850	1150	1160	1230
0.51	930	1130	1400	2830	1120	1140	1220
0.52	920	1110	1380	2810	1090	1130	1210

Table III. Thermal conductivity for different volume fractions of AlN powder, ϕ_p

Volume Fraction (ϕ_p)	Temperature (K)						
	315	336	356	377	397	417	436
	Thermal Conductivity (W/m·K)						
0	0.195	0.188	0.182	0.176	0.171	0.166	0.162
0.48	3.95	3.55	2.08	2.47	1.91	1.90	2.32
0.49	4.03	3.62	2.52	2.71	1.95	1.94	2.37
0.5	4.11	3.69	2.16	2.57	1.99	1.97	2.41
0.51	4.18	3.76	2.19	2.61	2.02	2.01	2.46
0.52	4.26	2.37	2.23	2.41	2.22	2.2	2.7

Specific Heat

The specific heat of powder–polymer mixtures has been estimated by different mixing rules.^{5–8} In this study, a model that has been successfully applied to mixtures with high volume fraction fillers⁶ was used as shown in Eq. 4.

$$C_{p_c} = [C_{p_b}X_b + C_{p_p}X_p] * [1 + A * X_bX_p] \quad (4)$$

where C_p is the specific heat, X is the mass fraction, and the subscripts c, b, and p stand for the composite, binder, and powder, respectively. The parameter A is a correction factor assumed to be 0.2 for spherical particles. The mass fractions were calculated using Eq. 3. The specific heat values calculated for different volume fractions of powder at various temperatures are shown in Table II. The specific heat data for 0 and 0.52 volume fractions were experimentally obtained, while the values for intermediate volume fractions were estimated using Eq. 4. It was observed that the specific heat of the powder–polymer mixtures decreased with increasing volume fraction of powder. It was also observed that the specific heat increased with increase in temperature and reached a maximum at a transition temperature beyond which it again reduces. As

a specific example, a change of volume fraction from 0.48 to 0.52 at 374 K resulted in a decrease in specific heat from 1200 J/g K to 1130 J/g K. The data in Table II indicate that a $\pm 2.5\%$ change in specific heat results from a $\pm 4\%$ change in the volume fraction of AlN.

Thermal Conductivity

Several equations have been used to predict thermal conductivity of a composite at different filler concentrations.^{5,9,10} In this article, a general rule-of-mixtures model⁴ was used as represented in Eq. 5.

$$\lambda_c = \lambda_b\phi_b + \lambda_p\phi_p \quad (5)$$

where λ is the thermal conductivity, ϕ is the volume fraction of powder, and the subscripts c, b, and p stand for the composite, binder, and powder, respectively. The estimated values of thermal conductivity as a function of volume fraction of powder at various temperatures are shown in Table III. The thermal conductivity data for 0 and 0.52 volume fractions were experimentally obtained, while the data for intermediate volume fractions were estimated using Eq. 5. The values of thermal conductivity are similar to studies by Mamunya et al.¹¹

for AlN-epoxy composites at powder content of 0.4–0.5 volume fractions. The thermal conductivity increases with an increase in volume fraction of AlN powder, ϕ_p . Additionally, a decrease in the thermal conductivity value is observed when the temperature increases above glass transition. The data presented in Table III indicate that a $\pm 4\%$ variation in thermal conductivity results from a $\pm 4\%$ change in volume fraction of AlN.

Coefficient of Thermal Expansion

The coefficient of thermal expansion (CTE) of powder-polymer mixtures can be calculated by several models.^{8,9,12,13} In this paper, a first-order model was used,⁹ as shown in Eq. 6, since fewer empirical constants were required.

$$\alpha_c = X_p \alpha_p + \alpha_b (1 - X_p) \quad (6)$$

where, α is the thermal expansion coefficient, X is the mass fraction of the powder and the subscripts c, p and b stand for composite, powder and binder respectively. The CTE data are as shown in Table IV. The CTE data at 0 and 0.52 volume fractions AlN were experimentally obtained, while the rest were estimated using Eq. 6. It can be seen that the CTE value decreases with an increase in volume fraction of AlN. Typically, in the range of 0.48–0.52 volume fractions ϕ_p , the CTE varied between $2.28E-5 \text{ K}^{-1}$ and $2.18E-5 \text{ K}^{-1}$, which represents a $\pm 3\%$ variation in CTE for a $\pm 4\%$ change in volume fraction of AlN in the powder-polymer mixtures.

Elastic and Shear Modulus

In this paper, the Voigt model⁹ was used to predict the elastic and shear modulus as shown in Eq. 7.

$$E_c = E_p X_p + E_b (1 - X_p) \quad (7)$$

where E is the elastic or shear modulus and subscripts c, p, and b represent composite, powder, and binder, respectively. X is the mass fraction and is calculated using Eq. 3. Table V shows the elastic and shear modulus values estimated at different volume fractions of powder. The modulus data for powder volume fractions of 0 and 0.52 were experimentally obtained, while the values for the intermediate volume fractions were estimated using

Eq. 7. It can be seen that the elastic and shear modulus values increase with an increase in volume fractions of AlN. Typically, in the range of 0.48–0.52 volume fractions ϕ_p , the elastic modulus increased from $\sim 13000 \text{ MPa}$ to $\sim 14000 \text{ MPa}$, and the shear modulus varies between 4900 MPa and 5240 MPa , which represents a $\pm 3.5\%$ variation in the elastic and shear modulus for a $\pm 4\%$ change in volume fraction of AlN in the powder-polymer mixtures.

Viscosity

The viscosity of powder-polymer mixtures at different volume fractions of AlN can be predicted using numerous mixing rules.^{4,14–16} In this article, a simplified Krieger-Dougherty¹⁶ viscosity model was used as it is suitable for predicting viscosity values at higher volume fractions of powder using the fewest empirical constants, as given in Eq. 8.

$$\eta_c = \frac{\eta_b}{\left[1 - \frac{\phi_p}{\phi_{\max}}\right]^2} \quad (8)$$

where η and ϕ_p represent the viscosity and the volume fraction of powder, respectively, while the subscripts c and b represent composite and binder, respectively. The parameter ϕ_{\max} stands for the maximum packing fraction of the powder. Additionally, the Cross-WLF model¹⁷ was used to model the viscosity dependence of any given powder-polymer mixture on shear rate as shown in Eq. 9.

$$\eta = \frac{\eta_0}{1 + \left(\frac{\eta_0 \dot{\gamma}}{\tau^*}\right)^{1-n}} \quad (9)$$

where η is the melt viscosity (Pa s), η_0 is the zero shear viscosity, $\dot{\gamma}$ is the shear rate (1/s), τ^* is the critical stress level at the transition to shear thinning as determined by curve fitting, and n is the power law index in the high shear rate regime, which is also determined by curve fitting. The temperature dependence of viscosity of any powder-polymer mixture¹⁷ can be calculated using Eq. 10.

$$\eta_0 = D_1 \exp \left[-\frac{A_1 (T - T^*)}{A_2 + (T - T^*)} \right] \quad (10)$$

where T is the temperature (K). T^* , D_1 , and A_1 are curve-fitted coefficients. Additionally, A_2 is the WLF

Table IV. Coefficient of thermal expansion for different volume fractions of AlN powder, ϕ_p

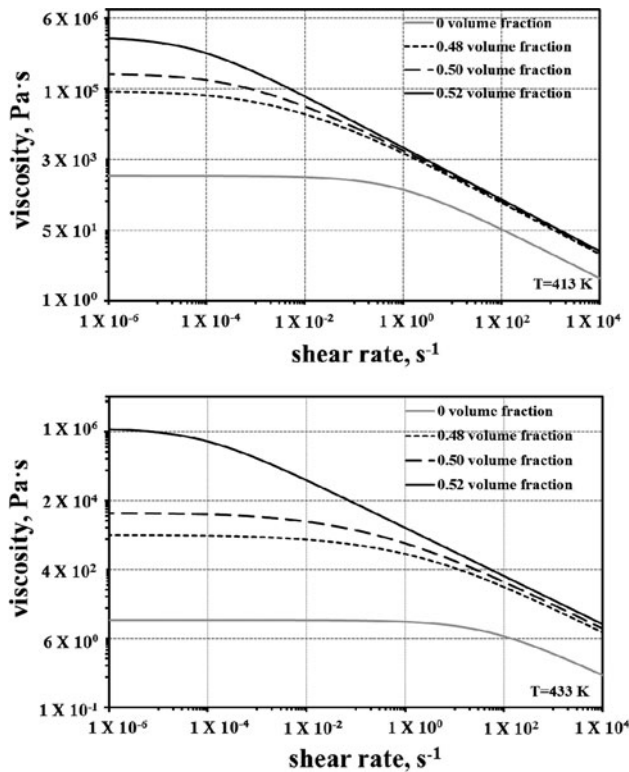
Volume Fraction (ϕ_p)	CTE (K^{-1})
0	$5.65E-05$
0.48	$2.28E-05$
0.49	$2.25E-05$
0.5	$2.23E-05$
0.51	$2.20E-05$
0.52	$2.18E-05$

Table V. Elastic and shear modulus values for different volume fractions of AlN powder, ϕ_p

Volume Fraction (ϕ_p)	Elastic Modulus (MPa)	Shear Modulus (MPa)
0	2560	930
0.48	13050	4900
0.49	13270	5000
0.5	13480	5070
0.51	13700	5150
0.52	13920	5240

Table VI. Cross-WLF constants for different volume fractions of AlN powder, ϕ_p

Cross WLF Constants	Volume Fraction (ϕ_p)					
	0	0.48	0.49	0.5	0.51	0.52
n	0.4	0.46	0.46	0.45	0.43	0.38
τ^* (Pa)	793.46	280.12	230.58	183.65	148.20	117.77
D_1 (Pa s)	$4.29E+23$	$8.73E+10$	$9.66E+10$	$1.81E+11$	$8.46E+10$	$8.78E+10$
T^* (K)	333	375.15	374.68	372.29	370.45	263.15
A_1	78.13	31.13	31.12	30.24	26.13	14.23
A_2 (K)	51.6	51.6	51.6	51.6	51.6	51.6


 Fig. 3. Comparison of viscosity with shear rate at 413 K and 433 K for different volume fractions of AlN powder, ϕ_p .

constant and is assumed to be 51.6 K. The values of these coefficients were obtained by curve fitting the estimated viscosity for different volume fractions of powder at various shear rates and temperatures and are summarized in Table VI. Figure 3 shows the shear-rate dependence of viscosity for several powder–polymer mixtures at 413 K and 433 K. The zero-shear viscosity was estimated from the plateau region at low shear rate, while the power law index was obtained from the slope at higher shear rates. The data for powder volume fractions of 0 and 0.52 are experimental values, while the data for intermediate volume fractions of powder were estimated from Eq. 8. It can be observed that the zero-shear

viscosity increased considerably with small increases in volume fraction ϕ_p in the range of interest. The curve-fitted WLF parameters n , τ^* , D_1 , T^* , A_1 , and A_2 were estimated for temperatures between 413 K and 433 K. The values estimated for n and τ^* for each temperature were then averaged out for individual volume fractions of powder, which resulted in an error of $\pm 1.5\%$. The values for the rest of the parameters did not vary with an increase in temperature. The power law index n decreased from 0.46 to 0.38 with an increase in volume fractions from 0.48 to 0.52. Similarly, τ^* decreased from 280 MPa to 118 MPa with an increase in volume fractions from 0.48 to 0.52. T^* is the transition temperature at which the material exhibits a change from Newtonian to shear-thinning behavior on increasing shear rates. It was observed that the value of T^* decreased from 370 K to 263 K when the volume fraction of AlN was changed from 0.51 to 0.52. It was also observed that A_1 changed from 31 to 14 when the volume fraction of AlN was changed from 0.48 to 0.52.

Specific Volume

The specific volume was calculated using the general rule-of-mixtures⁴ given in Eq. 11.

$$v_c = X_p v_p + v_b (1 - X_f) \quad (11)$$

where v is the specific volume, X is the mass fraction of the powder, and the subscripts c, p, and b refer to the composite, powder, and binder, respectively. The injection-molding software platform uses the two-domain Tait¹⁸ equation (Eq. 12) for generating viscosity values at different volume fractions of powder.

$$v(T, p) = v_o(T) \left[1 - C \ln \left(1 + \frac{p}{B(T)} \right) \right] + v_t(T, p) \quad (12)$$

where $v(T, p)$ is the specific volume at a given temperature and pressure, v_o is the specific volume at zero gauge pressure, T is temperature in K, p is pressure in Pa, and C is a constant assumed as 0.0894. The parameter B accounts for the pressure sensitivity of the material and is separately defined

Table VII. Dual-domain Tait constraints for different volume fractions of AlN Powder, ϕ_p

Dual-Domain Tait Constants	Volume Fraction (ϕ_p)					
	0	0.48	0.49	0.5	0.51	0.52
b5 (K)	336.15	331	331	331	331	331
b6 (K/MPa)	1.47E-07	1.65E-07	1.65E-07	1.65E-07	1.65E-07	1.65E-07
b1m (m ³ /kg)	0.001255	5.07E-04	5.00E-04	4.95E-04	4.90E-04	4.84E-04
b2m (m ³ /kg K)	1.34E-06	3.37E-07	3.27E-07	3.18E-07	3.09E-07	2.99E-07
b3m (Pa)	1.26E+08	2.71E+08	2.71E+08	2.71E+08	2.87E+08	2.87E+08
b4m (K ⁻¹)	0.005867	4.88E-03	4.88E-03	4.88E-03	2.49E-03	4.82E-03
b1s (m ³ /kg)	0.00117	4.92E-04	4.84E-04	4.75E-04	4.74E-04	4.69E-04
b2s (m ³ /kg K)	8.57E-07	1.82E-07	1.71E-07	1.65E-07	1.47E-07	9.70E-08
b3s (Pa)	2.40E+08	5.79E+08	5.79E+08	5.79E+08	5.79E+08	5.79E+08
b4s (K ⁻¹)	0.004155	1.26E-03	1.26E-03	1.26E-03	1.26E-03	1.26E-03
b7 (m ³ /kg)	8.46E-05	3.23E-06	7.78E-06	1.04E-05	7.27E-06	1.49E-05
b8 (K ⁻¹)	0.06688	4.50E-02	3.99E-02	1.85E-02	5.33E-02	1.10E-01
b9 (Pa ⁻¹)	1.39E-08	2.12E-08	2.12E-08	2.12E-08	2.12E-08	2.12E-08

for the solid and melt regions. For the upper bound¹⁸ when $T > T_t$ (volumetric transition temperature), B is given by Eq. 13.

$$v_o = b_{1m} + b_{2m}(T - b_5)B(T) = b_m e^{[-b_{4m}(T - b_5)]v_t(T, p)} = 0 \quad (13)$$

where, b_{1m} , b_{2m} , b_{3m} , b_{4m} , and b_5 are curve-fitted coefficients. For the lower bound,¹⁸ when $T < T_t$, the parameter B is given by Eq. 14.

$$-b_{4s}(T - b_5)v_t(T, p) = b_7 e^{[b_s(T - b_5) - b_9 p]} \quad (14)$$

where b_{1s} , b_{2s} , b_{3s} , b_{4s} , b_5 , b_7 , b_8 , and b_9 are curve-fitted coefficients. The dependence of the volumetric transition temperature T_t on pressure can be given by $T_t(p) = b_5 + b_6(p)$, where b_5 and b_6 are curve-fitted coefficients. The values of these coefficients are summarized in Table VII. Figure 4 shows the comparative plot of specific volumes at 0 MPa, 100 MPa, and 200 MPa pressure. The PVT behavior for 0.52 volume fraction of powder is plotted from experimental values while the data for 0.48 and 0.50 volume fractions of powder were estimated using Eq. 12. It can be observed that the specific volume increases with an increase in volume fraction of AlN. The dual-domain Tait constants were estimated using curve fitting for 0 MPa, 50 MPa, 100 MPa, 150 MPa, and 200 MPa pressure for volume fractions of 0 AlN, and 0.48 AlN to 0.52 AlN. The parameters b_5 , b_6 , and b_9 did not vary in the range of 0.48–0.52 volume fractions of AlN. It was also observed that the parameters, b_{1m} , b_{2m} , b_{1s} , and b_{2s} decreased on increasing the volume fractions from 0.48 to 0.52, but the change was nominal. The parameters b_{3m} , b_{4m} , b_{3s} , and b_{4s} also did not vary for volume fractions between 0.48 and 0.52. Parameters, b_7 and b_8 , showed a relatively greater sensitivity to changes in the volume fraction of AlN, however no distinctive trends could be observed.

SIMULATION RESULTS

Simulations were conducted for 0.48–0.52 volume fractions of AlN at 433 K melt temperature and 303 K mold temperatures using the heat-sink geometries shown in Fig. 5. The simulations were done for mold filling and packing stages. The progressive filling behavior of the feedstock with 0.51 volume fraction AlN is shown in Fig. 6 for the two geometries. It can be seen that the fin region of the mold cavity fills at the end of the molding stage.

Figure 7 shows the variation of part weight as a function of volume fraction of AlN for the two heat-sink geometries shown in Fig. 5. The part weight increases with an increase in volume fraction of AlN powder from 0.48 to 0.52. This increase in part weight with an increase in powder volume fraction can be attributed to an increase in density values with a rise in volume fractions of AlN as observed in Table I. Furthermore, for an AlN powder volume fraction change from 0.48 to 0.52, the part weight changes from 0.35 to 0.38 g for heat-sink substrate without fins. In the case of the heat-sink substrate with fins, the corresponding change is from 0.69 to 0.76 g. This change denotes a $\pm 3\%$ variation in part weight for a $\pm 4\%$ change in the volume fraction of AlN. It was also observed that the part weight doubled for heat-sink substrate with fins (Fig. 5b) in comparison to the heat-sink substrates without fins (Fig. 5a).

As the filling phase nears completion, the packing phase commences during which the part cools until a 100% frozen volume is obtained. Figure 8 shows the dependence on freeze time on the volume fraction of AlN powder in the feedstock. It can be observed from Fig. 8 that for a change of 0.48–0.52 volume fractions of AlN, the freeze time changes from 2.2 s to 1.6 s for heat-sink substrate without fins. In the case of the heat-sink substrate with fins, the change in freeze time is from 2.6 s to 1.6 s. This

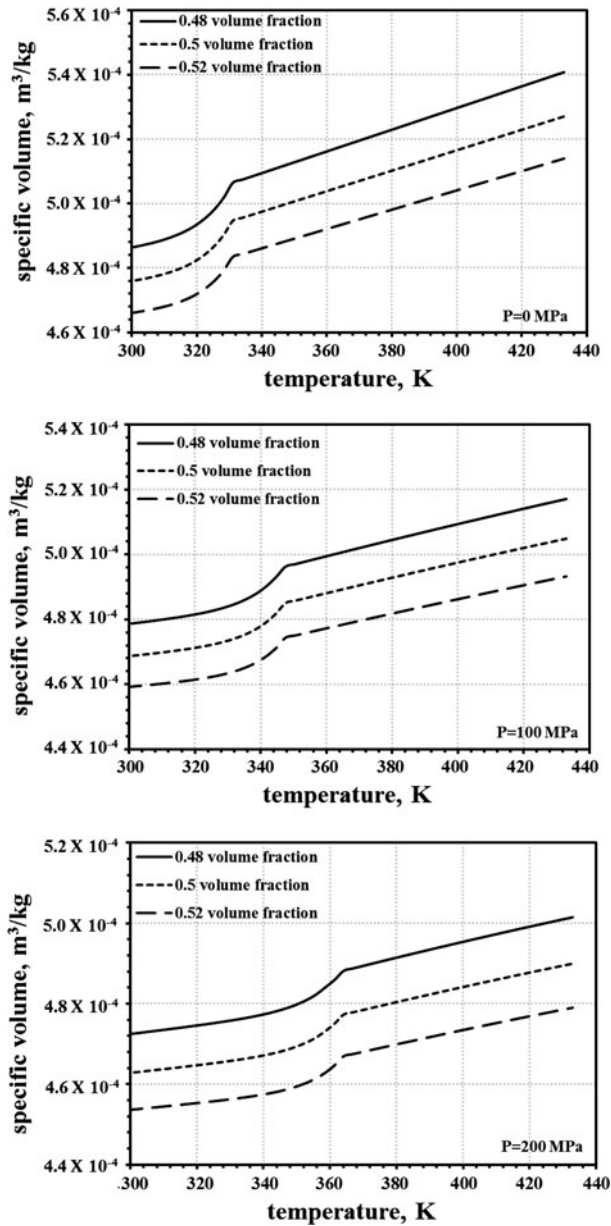


Fig. 4. PVT for 0 MPa, 100 MPa, and 200 MPa pressure at different volume fractions of AlN powder, ϕ_p .

denotes a $\pm 2.5\%$ variation in freeze time for a $\pm 4\%$ change in the volume fraction of AlN. The change in freeze time as a function of volume fraction can be attributed to the change in thermal properties estimated from Eqs. 4 and 5.

Figure 9 shows the variation in peak injection pressure as a function of the volume fraction of powder for the two heat-sink substrates. The peak injection pressure is located near the gate of the mold cavity. The peak injection pressure is relatively higher for the heat-sink substrate with fins compared to the heat-sink substrate without fins as a result of an increase in volumetric flow rate. It can be seen that for the heat-sink substrate with fins, the peak injection pressure increases from ~ 14 MPa to ~ 16 MPa with an increase in powder volume fraction from 0.48 to 0.52. This behavior can be attributed to an increase in the viscosity of the powder–polymer mixture as represented in Eqs. 8–10. An increase in injection pressure directly increases the clamp force and correspondingly reduces the number of mold cavities that can be simultaneously filled on a molding machine. An increase in injection pressure can also result in an undesirable alteration of the melt flow such as jetting. Furthermore, microstructural inhomogeneity can also be introduced in the part at higher injection pressures due to powder–polymer separation.

Figure 10 shows the dependence of volumetric shrinkage of the heat-sink substrates as a function of powder volume fraction. It can be seen that the volumetric shrinkage generally decreases from $\sim 8.5\%$ to $\sim 7\%$ with increase in powder volume fraction from 0.48 to 0.52. This can be attributed to the PVT behavior of the powder–polymer mixtures as described in Eqs. 11–14.

Figure 11 shows the weld-line distribution for the two heat-sink substrates as a function of powder volume fraction. No significant differences were observed (Fig. 11a and b) for the weld-line distributions in the heat-sink substrate without fins as the powder volume fraction increased from 0.48 to 0.52. In contrast, a number of new weld lines

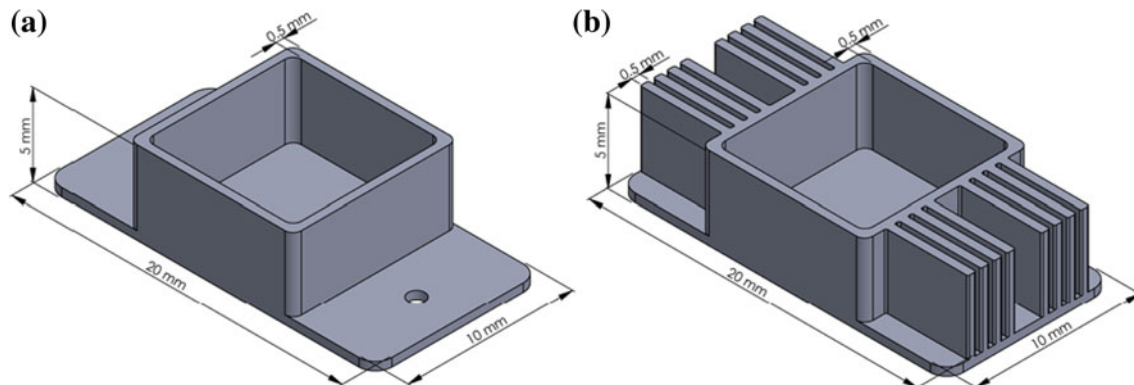


Fig. 5. Mold geometry used in injection-molding simulations: (a) simple heat-sink substrate without fins and (b) heat-sink substrate with fins.

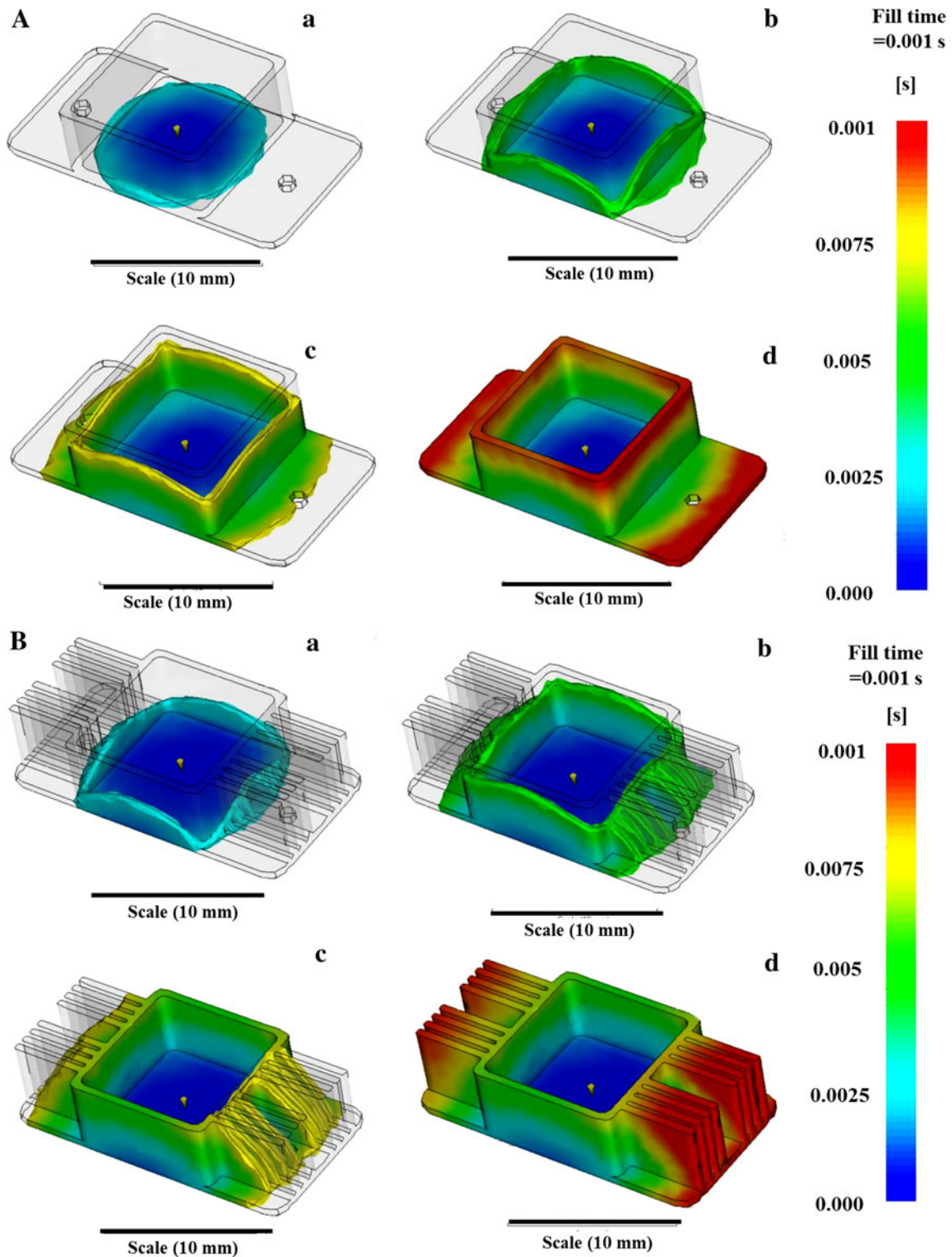


Fig. 6. (A) Progressive filling of the heat-sink substrate without fins shown in Fig. 5a. (B) Progressive filling of the heat-sink substrate with fins shown in Fig. 5b.

appeared in the fin region of the second heat-sink substrate (Fig. 11c and d) when the powder volume fraction increased from 0.48 to 0.52. Thus, as the

part complexity increases, the sensitivity of defect evolution to changes in material composition can increase. Further analysis on the strength of the

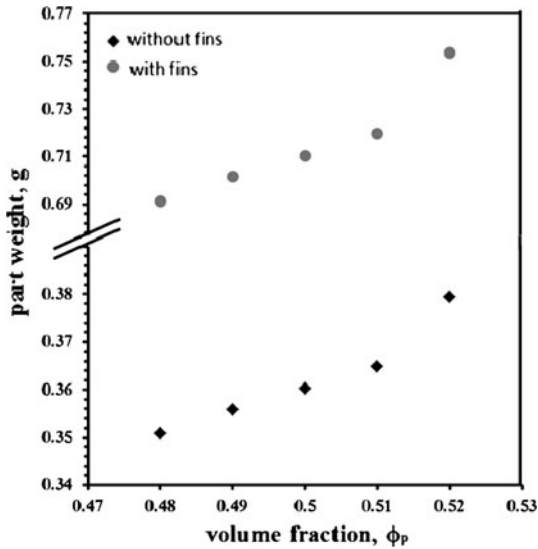


Fig. 7. Part weight at different volume fractions of AIN powder, ϕ_p .

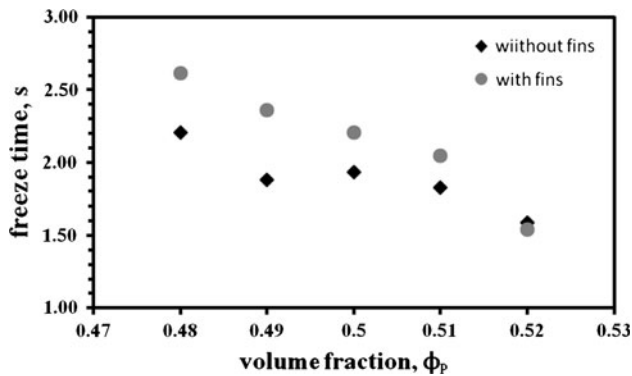


Fig. 8. Freeze time at different volume fractions of AIN powder, ϕ_p .

weld lines as well as residual stresses in the molded parts will be performed in the future, based on the data in Eqs. 6 and 7.

CONCLUSIONS

The thermal, rheological, and PVT properties of powder–polymer mixtures can be modeled as a

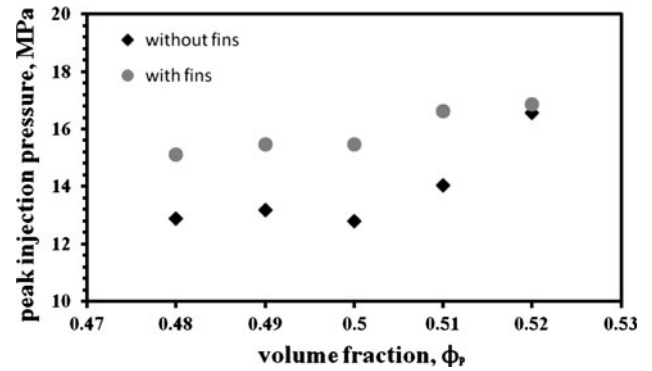


Fig. 9. Pressure at injection location at different volume fractions of AIN powder, ϕ_p .

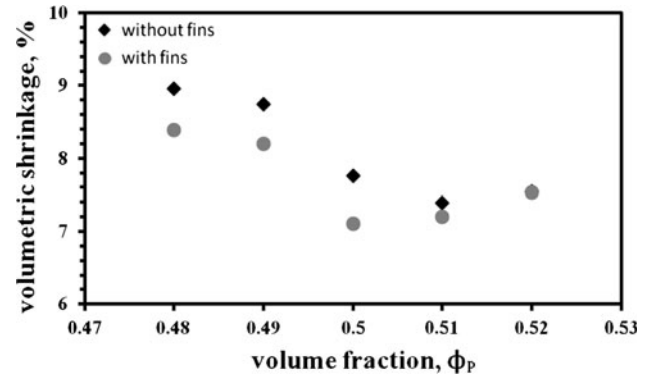


Fig. 10. Volumetric shrinkage, percentage at different volume fractions of AIN powder, ϕ_p .

function of powder volume fraction in the concentration ranges of interest to PIM. This data is critical to understanding the consequences of material composition on the mold-filling behavior of powder–polymer mixtures. The combination of experimental methods, constitutive models, and the computer simulation platform analyzed in this article represents a useful approach to address problems of precision and defects in PIM parts early in the design cycle. It is anticipated that the approach presented in this article will avoid expensive and

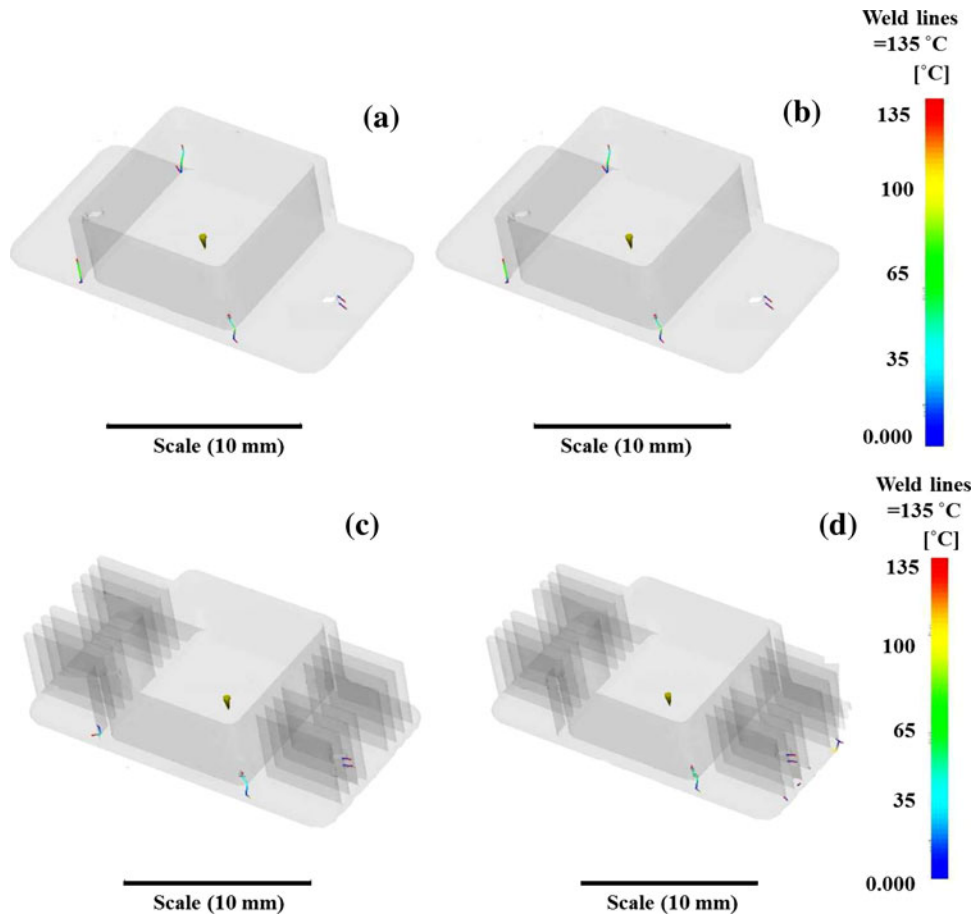


Fig. 11. Weld-line distribution in the heat-sink geometries without fins (top) and with fins (bottom), at 0.48 (a and c) and 0.52 (b and d) volume fractions of AlN powder, ϕ_p .

time-consuming, trial-and-error iterations currently prevalent in PIM.

ACKNOWLEDGMENT

The authors would like to acknowledge financial support from the National Science Foundation (Award # CMII 1200144).

REFERENCES

1. R.M. German and S.J. Park, *Mathematical Relations in Particulate Materials Processing: Ceramics, Powder Metals, Cermets, Carbides, Hard Materials, and Minerals* (New York: John Wiley & Sons, 2008).
2. V.P. Onbattuvelli, S. Vallury, T. McCabe, S.J. Park, and S. Atre, *Powder Inject. Mould. Int.* 4, 64 (2010).
3. J. Chen, J.-G. Mi, and K.-Y. Chan, *Fluid Phase Equilib.* 178, 87 (2001).
4. L.E. Nielsen, *Predicting the Properties of Mixtures: Mixture Rules in Science and Engineering* (New York: Marcel Dekker, 1978).
5. T. Zhang, J.R.G. Evans, and K.K. Dutta, *J. Eur. Ceram. Soc.* 5, 303 (1989).
6. D.T. Jamieson and G. Cartwright, *Properties of Binary Liquid Mixtures: Heat Capacity* (East Kilbride, Scotland: National Engineering Laboratory, 1978).
7. R.K. Sinnott, J.M. Coulson, and J.F. Richardson, *Chemical Engineering Design* (Waltham: Butterworth-Heinemann, 2005).
8. C.J. Cremers and H.A. Fine, *Thermal Conductivity* (New York: Springer, 1991).
9. C.P. Wong and R.S. Bollampally, *J. Appl. Polym. Sci.* 74, 3396 (1999).
10. Y. Zhang, Z. Shen, and Z. Tong, *Electronic Packaging Technology, 2007* (New York: IEEE, 2007), p. 1.
11. Y.P. Mamunya, *Eur. Polym. J.* 38, 1887 (2002).
12. T. Zhang and J.R.G. Evans, *J. Eur. Ceram. Soc.* 6, 15 (1990).
13. S. Elomari, R. Boukhili, and D.J. Lloyd, *Acta Mater.* 44, 1873 (1996).
14. T. Zhang and J.R.G. Evans, *J. Eur. Ceram. Soc.* 5, 165 (1989).
15. P.C. Hiemenz and R. Rajagopalan, *Principles of Colloid and Surface Chemistry* (Boca Raton: CRC Press, 1997).
16. V.P. Onbattuvelli, "The Effects of Nanoparticle Addition on the Processing, Structure and Properties of SiC and AlN" (Ph.D. Thesis/Dissertation, Oregon State University, 2010).
17. X.Z. Shi, M. Huang, Z.F. Zhao, and C.Y. Shen, *Adv. Mater. Res.* 189–193, 2103 (2011).
18. H.H. Chiang, C.A. Hieber, and K.K. Wang, *Polym. Eng. Sci.* 31, 116 (1991).